IEEE Access
Multidisciplinary | Rapid Review | Open Access Journal

Received July 5, 2017, accepted July 13, 2017, date of publication July 26, 2017, date of current version August 14, 2017.

Digital Object Identifier 10.1109/ACCESS.2017.2731998

Time-Varying Model-Based Observer for Marine Surface Vessels in Dynamic Positioning

SVENN ARE VÆRNØ[1], ASTRID H. BRODTKORB[1], ROGER SKJETNE[1], AND VINCENZO CALABRÒ[2], (Member, IEEE)

[1]Centre of Autonomous Marine Operations and Systems, Department of Marine Technology, Norwegian University of Science and Technology, 7491 Trondheim, Norway
[2]Kongsberg Maritime AS, 3616 Kongsberg, Norway

Corresponding author: Svenn Are Værnø (svenn.are.varno@ntnu.no)

This work was supported in part by the Research Council of Norway, through the Centre of Excellence NTNU AMOS, under Project 223254, and through the Centre for Research-based Innovation MOVE, under Project 237929.

ABSTRACT This paper deals with the problem of transient events in model-based observers for dynamic positioning of marine surface vessels. Traditionally, model-based observers experience a deterioration of performance during transients, and there is a give or take relationship between transient and steady state performance. To remedy this problem, we propose to use time-varying gains for a model-based observer. The gains are aggressive during transients to improve transient performance, and relaxed in steady state to lower the oscillations of the estimates. The proposed observer is analyzed with regard to stability. Its performance is verified in both a high-fidelity simulation model, and on experimental data with the research vessel (R/V) Gunnerus. In addition, a partial closed-loop validation with R/V Gunnerus has been performed.

INDEX TERMS Dynamic positioning, Marine control systems, Observers.

I. INTRODUCTION

A dynamically positioned (DP) vessel means a unit or a vessel which automatically maintains its position (fixed location or predetermined track) exclusively by means of thruster force [1]. As dynamic positioning operations are moving into harsher conditions or doing more complex operations, better transient performance of the DP system is required. A bias term is used as integral action to model slowly-varying environmental loads and unmodeled dynamics, and for good model-based observer performance it is important to estimate this bias accurately. Integral action is typically based on the assumption that this bias is constant. The bias load is, however, slowly-varying in steady state, but can vary rapidly in transient events. A major obstacle in transient performance of DP is how to handle rapid changes in this bias load.

In model-based observers for DP, the environmental loads are typically modeled as a constant force vector in the North-East-Down-frame (NED), that is, the following kinetic equation is typically used, $M\dot{\nu} = -D\nu + R(\psi)^\top b + \tau$, where b is this constant load (bias) vector in the NED-frame and R(·) is a rotation matrix mapping into the body-frame of the vessel; see Section II-A for more details about the modeling, as well as [2], [3]. There are instances when the bias loads change significantly over a short time period, where this assumption does not hold. In Figure 1 we investigate, as an example, how the current and wave drift loads vary in the NED-frame over a heading change. The figure shows a high-fidelity simulation of a surface vessel performing two maneuvers; first, a position setpoint change, and afterwards, a combined setpoint change of position and heading. In the top plot of Figure 1 the low-frequency North position and heading angle are shown. In the bottom plot the combined current and wave-drift loads are shown in North and yaw. We observe that the loads experienced by the vessel in the NED-frame changes significantly, even though the current and wave parameters are constant in the NED-frame. This is because the forces experienced by the vessel vary due to ship hull geometry, which is not accounted for in the simple (but effective) bias model. Consequently, for some time after a transient event, the bias load estimate of a model-based observer will be off, leading to poor velocity and position estimates. This example clearly illustrates that if the vessel changes heading, the common slowly-varying assumption of the bias model in the NED-frame does not apply in transients; see also [4] for a discussion on this for AUVs (Autonomous Underwater Vehicles) exposed to currents. Other common occurrences of rapid bias load changes include wave trains, rotational currents, sea-ice loads, or during mode changes in the operation of the DP system.

Even with the knowledge that the slowly-varying bias assumption is not good in transients, it is difficult to device better ways of handling this. One non-model based option

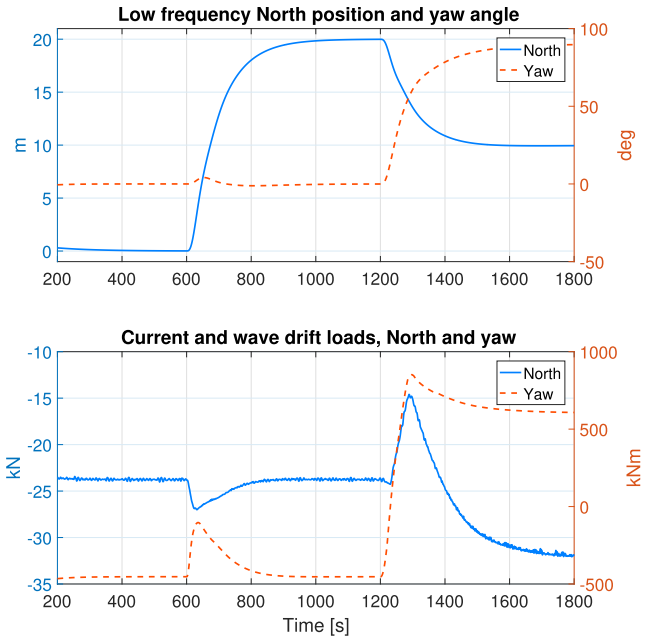

FIGURE 1. Low-frequency North position and heading angle (top), and current and wave-drift loads in North and yaw experienced by the vessel (bottom).

is to measure accelerations to estimate the forces in a direct fashion as suggested in [5]. Another option that does not require more instrumentation is to use a more complex model of the hydrodynamic loads, but this would also give a more complex control algorithm that could be more difficult to parameterize and analyze with respect to stability. Moreover, depending on the type of environment, there will always be uncertainty in such models.

There exists other time-varying observer schemes for DP in the literature. See for instance [6], where an inertial observer for DP is proposed that uses time-varying gains to improve convergence and suppress sensor noise. In [7] and [8] a wave encounter frequency observer is proposed, where time-varying gains are used in an adaption law, and in [9] hybrid gains are used in integral action for DP.

The main contribution of this paper is to construct a model-based observer with time-varying gains that performs well in transients as well as in steady state. In state-of-the-art fixed gain model-based observer design for DP [2], there is a tradeoff in tuning the observer for either good steady state performance or good transient performance, and in commercial systems there are typically three gain settings; low, medium, and high, which the DP operator can select from. As an extension of the observer design from [10], we propose in this paper to use time-varying bias and velocity injection gains. The paper includes a comprehensive analysis and thorough selection of gains, and an observer verification based on experimental data. Another contribution is a full-scale closed-loop validation of the observer when conducting a DP experiment on the AMOS DP Research Cruise 2016 [11]. Demonstration of the observer performance through full-scale closed-loop experiments on an academic research cruise is, to the author's knowledge, not done before.

Notation and Terminology: In UGES, G stands for Global, U for uniform, E for exponential, and S for Stable. The smallest and largest eigenvalues of a matrix $A \in \mathbb{R}^{n\times n}$ is $\lambda_{min}(A)$ and $\lambda_{max}(A)$, respectively, and $\mathbb{R}_{>0}$ denotes positive real numbers. The $\mathcal{L}_\infty$ signal norm is $\|x\|_\infty = \text{ess sup}\{|x(t)| : t \geq 0\}$.

II. PROBLEM FORMULATION

In the following we separate between the *simulation model*, which is a high-fidelity model used for control and observer verification, and the *control design model*, which is a simplified model intended for control and observer design. The control design model typically only includes the parts relevant for the operational regime of the observer or controller. For low-speed applications such as DP, this implies that the Coriolis and centripetal forces are neglected, and the nonlinear damping is typically neglected as well. See [3], and [2] for DP modeling details, and [12], [13], [14] for other insightful DP literature.

Two reference frames are used: The North-East-Down frame (NED) is a local Earth-fixed frame assumed non-rotating, with x-axis pointing North, y-axis pointing East, and z-axis pointing down to the center of the Earth. The body-frame is a local frame, centered along the center line and in the water plane of the vessel. The x-axis points in the direction of the the bow, y-axis starboard, and z-axis down.

A. CONTROL DESIGN MODEL

The control design model is a 3 degree of freedom (DOF) model,

$$\dot{\xi} = A_w \xi + E_w w_w \tag{1a}$$
$$\dot{\eta} = R(\psi)\nu \tag{1b}$$
$$\dot{b} = -T_b^{-1} b + w_b \tag{1c}$$
$$M\dot{\nu} = -D\nu + R(\psi)^\top b + \tau \tag{1d}$$
$$y = \eta + C_w \xi + v_y, \tag{1e}$$

where there is a separation between the first order wave-induced motion in (1a) and the low-frequency motion of the vessel in (1b) - (1d) [2]. When controlling the vessel, we are typically only interested in the low-frequency part of the motion. Controlling the total motion causes extra wear and tear on the thrusters, and in most cases it is not possible to counteract the first order wave-induced motion. The wave-induced motion $\xi \in \mathbb{R}^5 \times \mathbb{S}^1$ is modeled by a second order mass-spring-damper model, where A_w is a Hurwitz matrix that contains the peak frequency of the sea state and the damping ratio of the wave motion model, $w_w \in \mathbb{R}^3$ is zero mean white noise, and $E_w = \begin{bmatrix} 0_{3\times 3} & I_{3\times 3} \end{bmatrix}^\top$. The vector $\eta := \text{col}\,(\eta_N, \eta_E, \psi) \in \mathbb{R}^2 \times \mathbb{S}$ contains the low-frequency North/East position and heading angle of the vessel, and the bias load $b := \text{col}\left(b_N, b_E, b_\psi\right) \in \mathbb{R}^3$ is a NED-fixed vector that contains the slowly-varying loads affecting the vessel due to wave drift, mean and slowly-varying currents, mean wind

loads, as well as unmodeled dynamics from inaccurate mass and added mass, unmodeled hydrodynamic effects, and errors in thrust modeling. The bias load dynamics are modeled by a Markov process, where T_b is a diagonal matrix of time constants, and $w_b \in \mathbb{R}^3$ is the white noise vector [2]. The vector $\nu = \text{col}\,(u, v, r) \in \mathbb{R}^3$ contains the low-frequency surge/sway velocity and yaw rate in the body frame of the vessel, $M \in \mathbb{R}^{3\times3}$ and $D \in \mathbb{R}^{3\times3}$ are the mass (inertia and added mass) and linear damping matrices, respectively. $\tau \in \mathbb{R}^3$ is the control vector. The measurement vector $y \in \mathbb{R}^3$ is a sum of the low-frequency North/East position and heading η, and the wave frequency North/East and heading $C_\omega \xi$, where $C_\omega = \begin{bmatrix} 0_{3\times3} & I_{3\times3} \end{bmatrix}$, and the measurement noise vector $v_y \in \mathbb{R}^3$. The rotation matrix $R(\psi)$ rotates a 3 DOF vector from the body to the NED frame. It satisfies $R(\psi)R(\psi)^\top = I$ and $\det(R(\psi)) = 1$, and its time derivative is $\dot{R} = R(\psi)Sr$, where

$$R(\psi) = \begin{bmatrix} \cos(\psi) & -\sin(\psi) & 0 \\ \sin(\psi) & \cos(\psi) & 0 \\ 0 & 0 & 1 \end{bmatrix}, \quad S = \begin{bmatrix} 0 & -1 & 0 \\ 1 & 0 & 0 \\ 0 & 0 & 0 \end{bmatrix}; \tag{2}$$

see [2] and [15] for details.

B. ASSUMPTIONS

Since the wave-induced heading angle is typically less than 1° for normal sea states and less than 5° for extreme sea states, we assume as in [16] that:

(A1) $R(\psi + \psi_w) \approx R(\psi)$, that is, the heading angle due to wave-induced motion, ψ_w, is small.

We also make the following assumptions:

(A2) The added mass part of M and the wave-induced damping of D are set to the values when the wave frequency approaches infinity, and therefore they are constant. In addition, starboard/port symmetry is assumed, $M = M^\top > 0$, and that the damping matrix satisfies $D + D^\top > 0$.

(A3) $w_w = w_b = 0$. Since the presented observers are deterministic, both the wave and the bias estimates in the observers are driven by the estimation error [16].

(A4) In the stability analysis, no measurement noise is considered, $v_y = 0$. However, simulation and experimental data include it.

The last two assumptions are common for a deterministic observer design, but in practice we will see that the resulting observer has good filtering properties of these noise inputs.

C. PROBLEM STATEMENT

We consider the case where the bias b is constant or slowly varying in long periods of time, but then sporadically experiences rapid changes due to some transient condition. The problem is thus to design an observer for (1) that accurately estimates the states during both steady and transient conditions. The performance of the observer shall be compared to a conventional design basis through a performance index.

III. OBSERVER DESIGN

The proposed observer is based upon the "nonlinear passive observer" initially presented in [16]. Time-varying injection gains for the velocity and the bias dynamics are proposed to capture slowly-varying dynamics in steady state, and fast dynamics during transients. The observer is designed by copying the control design model (1) and adding injection terms, that is,

$$\dot{\hat{\xi}} = A_w\hat{\xi} + K_1\tilde{y} \tag{3a}$$
$$\dot{\hat{\eta}} = R(\psi)\hat{\nu} + K_2\tilde{y} \tag{3b}$$
$$\dot{\hat{b}} = -T_b^{-1}\hat{b} + K_3(t)\tilde{y} \tag{3c}$$
$$M\dot{\hat{\nu}} = -D\hat{\nu} + R(\psi)^\top\hat{b} + \tau + K_4(t)R(\psi)^\top\tilde{y} \tag{3d}$$
$$\hat{y} = \hat{\eta} + C_w\hat{\xi}, \tag{3e}$$

where $\hat{\xi} \in \mathbb{R}^5 \times \mathbb{S}^1$, $\hat{\eta} \in \mathbb{R}^2 \times \mathbb{S}$, $\hat{b} \in \mathbb{R}^3$, and $\hat{\nu} \in \mathbb{R}^3$ are the state estimates, $K_1 \in \mathbb{R}^{6\times3}$, $K_2, K_3(t), K_4(t) \in \mathbb{R}^{3\times3}$ are non-negative gain matrices, and $\tilde{y} = y - \hat{y}$ is the measurement error. The gains K_1 and K_2 depend on the peak frequency of the wave spectrum as in [16]. The observer in (3) was preliminarily presented in [10] with only $K_3(t)$ varying with time. Further analysis shows that an appropriate choice of values for K_3 and K_4 are important for good transient observer performance, so here a scheme for time-varying K_3 and K_4 is proposed.

As discussed in Section I, the transient changes of the bias load experienced by the vessel pose challenges for the model-based observer in (3). To illustrate this, consider the following case: When the vessel is pushed off setpoint due to a rapid external load b, the DP controller will try to decelerate and stop the movement, and bring the vessel back to setpoint. The observer has information about this control action τ and position deviation $\tilde{y}$, whereas the bias observer state $\hat{b}$ underestimates the actual bias load. While the position deviation is helpful for the observer, the control action's "push back" to position is seen as an indication that the vessel is moving in the direction of the control action, which initially is opposite of the actual motion of the vessel. Therefore, including feedback control action deteriorates the observer performance in the initial phase of a transient.

Therefore, in order to achieve good transient observer performance, the injection gain $K_4(t)$ in the velocity dynamics (3d) must be high enough to dominate the feedback control action. In addition, the injection gain $K_3(t)$ in (3c) must be high enough in order for the bias estimate to more accurately track the bias load value during the transient. Keeping these gains high all the time will, however, result in oscillatory estimates of the bias and velocity in steady state.

$K_3(t)$ and $K_4(t)$ are proposed to stay within the range

$$K_i(t) \in [K_{i,min}, K_{i,max}], \quad i = 3, 4\ \forall t \geq t_0.$$

The values of $K_{i,max}$ should be set such that they give a good transient performance of the observer, and $K_{i,min}$ such that the observer performs well in steady state. The steady state tuning is purposely set low, providing calmer estimates to the controller, as is normal tuning practice for conventional DP observers. The time-varying gains should react quickly to transient events by approaching their maximum values rapidly.

The equation for $K_3(t)$ and $K_4(t)$ is thus proposed as

$$K_i(t) = \kappa(t)K_{i,max} + (1-\kappa(t))K_{i,min}, \quad i = 3, 4, \tag{4}$$

where $\kappa(t) \in [0, 1]$, $\forall t \geq 0$. Whenever there is a transient event, κ should approach 1, and whenever the vessel is in steady state, κ should stay close to 0.

Three transient events are considered. The first is an operator-executed heading change, which is easily detected through the desired yaw rate from the guidance system. The second is a change in the environmental disturbances. This is detected through a deterioration of the observer performance. The final transient is the error due to initialization of the observer. The proposed dynamics for κ is

$$\kappa(t) = \max\{0, \beta(t) - 1\}\} \tag{5a}$$
$$\beta(t) = \min\{\varepsilon_{r_d}|r_d(t)| + \varepsilon_\eta|\tilde{\eta}_f(t)|, 2\} \tag{5b}$$
$$\dot{\tilde{\eta}}_f = -T_{\eta_f}^{-1}\{\tilde{\eta}_f - \tilde{y}\}, \tag{5c}$$

where $\varepsilon_{r_d} \in \mathbb{R}_{>0}$ and the desired yaw rate $r_d(t) \in \mathbb{R}$ are related to a heading change. The second term $\tilde{\eta}_f$ in (5b) is the lowpass filter (5c) that tracks the observer output error performance, where $T_{\eta_f} \in \mathbb{R}^{3\times3}$ is a diagonal matrix of filter time constants. If the observer performance deteriorate, $|\tilde{\eta}_f|$ will grow. The time constants and $\varepsilon_\eta \in \mathbb{R}_{>0}$ are tuned such that κ approaches zero at steady state. To incorporate the effect of a transient at observer startup, $\tilde{\eta}_f$ is initialized with non-zero values. The value of β in (5b) takes a value between zero and two. The maximum function in (5a) defines a threshold such that κ will not go above zero before β is larger than one. This will reduce the amount of switching back and forth.

IV. STABILITY ANALYSIS

By defining the estimation error states $\tilde{\xi} := \xi - \hat{\xi}$, $\tilde{\eta} := \eta - \hat{\eta}$, $\tilde{\nu} := \nu - \hat{\nu}$, and $\tilde{b} := b - \hat{b}$, and subtracting the observer equations (3) from the control design model (1), we get the observer error dynamics,

$$\dot{\tilde{\xi}} = A_w\tilde{\xi} - K_1\tilde{y} \tag{6a}$$
$$\dot{\tilde{\eta}} = R(\psi)\tilde{\nu} - K_2\tilde{y} \tag{6b}$$
$$\dot{\tilde{b}} = -T_b^{-1}\tilde{b} - K_3(t)\tilde{y} \tag{6c}$$
$$M\dot{\tilde{\nu}} = -D\tilde{\nu} + R(\psi)^\top\tilde{b} - K_4(t)R(\psi)^\top\tilde{y}. \tag{6d}$$

The stability analysis follows the same structure as in [10]. However, the following proof removes the assumption of a maximum yaw rate. We collect all the observer error states from (6) in a vector $x := \text{col}(\tilde{\xi}, \tilde{\eta}, \tilde{b}, \tilde{\nu}) \in \mathbb{R}^{15}$ and write the observer error dynamics from (6) compactly as

$$\dot{x} = A(\psi, t)x, \tag{7}$$

where the equation can be derived, as shown at the bottom of this page.

The dynamics (7) can be written as [17],

$$\dot{x} = T(\psi)^\top A(0, t)T(\psi)x, \tag{8}$$

where

$$T(\psi) = \text{diag}\{R(\psi)^\top, R(\psi)^\top, R(\psi)^\top, R(\psi)^\top, I\}, \tag{9}$$

if the matrices K_2, $K_3(t)$, and T_b commute with $R(\psi)$, and $K_1\ R = \text{diag}\{R, R\}K_1$. Note that the nonlinearity $R(\psi)$ is replaced by $R(0) = I$ in $A(0, t)$. Moreover, it can be shown that we can write $A(0, t)$ as

$$A(0, t) = \kappa(t)A_{max} + (1-\kappa(t))A_{min}, \quad \kappa(t) \in [0, 1]. \tag{10}$$

where $A_{min} = A(0, 0)$ and $A_{max} = A(0, 1)$.

Proposition 1: The equilibrium $x = 0$ of (7) where $K_i(t)$, $i = 3, 4$, is given by (4), and

$$\kappa(t) \in [0, 1] \quad \forall t \geq 0,$$

is uniformly globally exponentially stable (UGES) if the following holds:

(1) The matrices K_2, $K_3(t)$, and T_b commute with the rotation matrix $R(\psi)$, and $K_1\ R = \text{diag}\{R, R\}K_1$.
(2) The linear matrix inequalities (LMIs) below are satisfied,

$$A_{min}^\top P + PA_{min} < -Q \tag{11a}$$
$$A_{max}^\top P + PA_{max} < -Q \tag{11b}$$
$$PS_T - S_TP \text{ is skew-symmetric}, \tag{11c}$$

where $S_T = \text{diag}\{S, S, S, S, 0\}$, and $P \in \mathbb{R}^{15\times15}$ and $Q \in \mathbb{R}^{15\times15}$ are symmetric positive definite matrices. □

Proof 1: Consider the transformation $z = T(\psi)x$ given by (9), and notice that $T(\psi)^{-1} = T(\psi)^\top$. From (8) we get

$$\begin{aligned}\dot{z} &= T(\psi)T(\psi)^\top A(0, t)z + \dot{T}(\psi)T(\psi)^\top z \\ &= A(0, t)z - rS_Tz,\end{aligned} \tag{12}$$

$$A(\psi, t) := \begin{bmatrix} A_w - K_1C_w & -K_1 & 0 & 0 \\ -K_2C_w & -K_2 & 0 & R(\psi) \\ -K_3(t)R(\psi)^\top C_w & -K_3(t)R(\psi)^\top & -T_b^{-1} & 0 \\ -M^{-1}K_4(t)R(\psi)^\top C_w & -M^{-1}K_4(t)R(\psi)^\top & -M^{-1}R(\psi)^\top & -M^{-1}D \end{bmatrix}.$$

where r is the yaw rate. We introduce a quadratic Lyapunov function $V(z) = z^\top Pz$ with P from (11), and take the time derivative of V along (12), which gives

$$\begin{aligned}\dot{V} &= z^\top\{PA(0,t) + A(0,t)^\top P - r(PS_T - S_T P)\}z \\ &= 0.85z^\top\{\kappa(t)(PA_{max} + A_{max}^\top P) \\ &\quad + (1-\kappa(t))(PA_{min} + A_{min}^\top P)\}z \\ &\leq -q_m|z|^2 \end{aligned} \tag{13}$$

where q_m is the smallest eigenvalue of Q from (11).

V. SETUP, RESULTS, AND DISCUSSION

The observer in (3) has been tested on the high-fidelity simulation model and on full-scale experimental data, described in sections V-A and V-B, respectively. For the experimental data we only have data sets with negligible waves, so the observer tested does not apply the wave filter. Hence, the observer used is (3b)-(3d) with $\hat{y} = \hat{\eta}$. In addition, the data series for the full-scale experiments contain a lot of transients, but little steady state. Therefore, the simulation study has a wider discussion of performance than the observer results on the experimental data.

After a presentation of the setup, we start with presenting a closed-loop verification of the observer from [10] onboard the R/V Gunnerus. This serves as a verification of the time-varying observer design, which is relevant for the observer presented in this paper, as the observers have similar structure and scheme for selecting the time-varying gains.

A. DP SIMULATION MODEL

The simulation model is a 6 DOF high-fidelity model of a platform supply vessel with main parameters shown in Table 1. The model includes nonlinear damping, Coriolis, centripetal forces, and linear damping, based on building blocks from the MSS Toolbox [18]. Wave drift and current forces are calculated using lookup tables, which give a realistic variation of the bias loads with vessel heading. Realistic noise is added to the measurement signals from the GPS and compass, with sampling rates of 1 Hz and 10 Hz, respectively.

TABLE 1. Simulation, platform supply vessel, and main parameters.

Parameters	Value
Length between perp.	80 m
Breadth	17.4 m
Draft	5.6 m
Displacment	6150 tons

The simulated sea state is very rough with significant wave height of 6 meters, and a peak frequency of 0.53 rad/s taken from the JONSWAP[1] spectrum. The mean incident wave heading is 190° (head waves) in the North/East frame [19]. The simulation also includes current with a speed of 0.5 m/s with direction of 160° (bow).

[1] Joint North Sea Wave Project

FIGURE 2. The NTNU-owned research vessel R/V Gunnerus.

TABLE 2. R/V Gunnerus, main parameters.

Parameters	Value
Length over all	31.3 m
Length between perp.	28.9 m
Breadth middle	9.6 m
Draft	2.7 m
Dead weight	107 tons

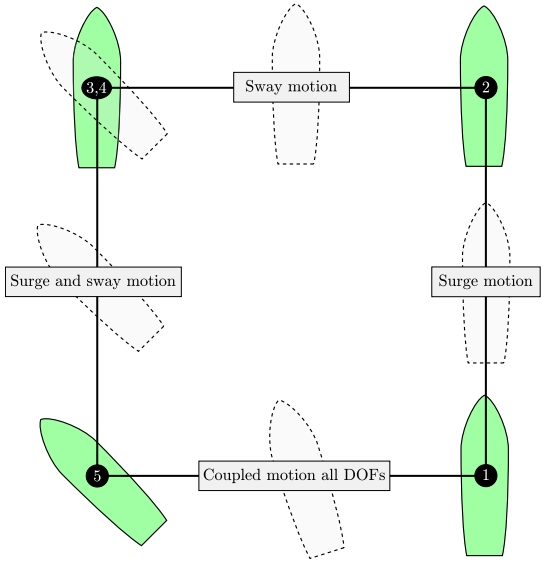

FIGURE 3. The 4-corner DP test. Courtesy: Øivind K. Kjerstad.

B. AMOS DP RESEARCH CRUISE 2016

Full-scale experimental data were collected during the AMOS DP Research Cruise (ADPRC) 2016 [11] with R/V Gunnerus, a 31-meter long research vessel owned and operated by NTNU, as seen in Figure 2, and with main parameters in Table 2. In addition, a closed-loop verification of the observer from [10] onboard the R/V Gunnerus was tested on the cruise. For the experimental data we only have data sets with negligible waves.

The data sets from the full-scale experiment with R/V Gunnerus are all from the vessel performing a box maneuver,

here called *DP 4-corner test*, as shown in Figure 3. The vessel starts at North and East position $(N, E) = (0, 0)$ with heading zero degrees, and the test steps are:

1) Position change to $(N, E) = (40m, 0)$ with zero heading (pure surge motion).
2) Position change 40 meter to $(N, E) = (40m, -40m)$ with zero heading (pure sway motion).
3) Heading change to $\psi = -45$ degrees (pure rotation).
4) Position change to $(N, E) = (0, -40m)$ keeping heading at -45 degrees (combined surge and sway motion).
5) Position change to $(N, E) = (0, 0)$ and heading $\psi = 0$ degrees (coupled motion with all DOFs).

C. PERFORMANCE EVALUATION

To compare performance of the different observer algorithms, we will apply the following cost functions as performance indicators,

$$J_\eta = \int_{t_0}^{t_f} \{|\eta_N - \hat{\eta}_N| + |\eta_E - \hat{\eta}_E| + \frac{180}{\pi}|\psi - \hat{\psi}|\}dt \quad (14a)$$

$$J_\nu = \int_{t_0}^{t_f} \{|u - \hat{u}| + |v - \hat{v}| + \frac{180}{\pi}|r - \hat{r}|\}dt \quad (14b)$$

$$J_b = \int_{t_0}^{t_f} \{\frac{|b_N - \hat{b}_N|}{\|b_N\|_\infty} + \frac{|b_E - \hat{b}_E|}{\|b_E\|_\infty} + \frac{|b_\psi - \hat{b}_\psi|}{\|b_\psi\|_\infty}\}dt, \quad (14c)$$

where t_0 and t_f are the initial and final time of the interval.

D. DERIVATIVE FREE OPTIMIZATION FOR TUNING

When comparing observers, a fair tuning is important. We would like to find the tuning based on optimization. Due to the absence of information about the gradient, Hessian, or higher derivatives of a typical cost function, a classic gradient descent-like method is not applicable. Therefore, derivative free optimization (DFO) will be used as a guide to tune the observers, and the MATLAB® function *fminsearch* has been adopted.

To illustrate how derivative free optimization works, let us consider a variable of interest, $x \in \mathbb{R}$. The goal is to establish a cost function to minimize the error $\tilde{x} = x - \hat{x}$ given a certain parameter $K \in \mathbb{R}$ and a simulation time of t_f seconds. We consider a cost function $J(K, t_f)$, where for each value of K a new simulation is performed and the cost function is evaluated. The derivative free optimization method explores the solution set around the current iteration result to compute a new solution point which minimizes the cost function. In our case this means to find a new value for K that gives a lower cost for J than the one before. There is a chance of getting stuck in a local minimum, and therefore several initial conditions for K are needed.

E. OBSERVER OF [10]: TIME-VARYING $K_3(t)$ ONLY, WITH FULL-SCALE CLOSED-LOOP VERIFICATION

The time-varying observer from [10] was tested in closed loop on the ADPRC 2016. The observer is similar to (3), with a time-varying bias injection gain $K_3(t)$, but K_4 was kept constant. However, since the waves were negligible while performing the closed-loop trials, the observer used in closed-loop was (3b)-(3d) with $\hat{y} = \hat{\eta}$.

The control law τ used for the full-scale experiments had a feedback term τ_{FB}, and a reference feedforward term τ_{FF}, where the feedback term consisted of a nonlinear PD (proportional, derivative) tracking term and a bias load rejection term,

$$\tau = \tau_{FB} + \tau_{FF} \quad (15a)$$

$$\tau_{FF} = M\dot{\nu}_d(t) + D\nu_d(t) \quad (15b)$$

$$\tau_{FB} = -K_p R(\psi)^\top(\hat{\eta} - \eta_d(t)) - K_d(\hat{\nu} - \nu_d(t)) - R(\psi)^\top \hat{b}_f, \quad (15c)$$

where K_p and K_d are positive definite gain matrices, and $\eta_d(t)$, $\nu_d(t)$, $\dot{\nu}_d(t)$ are the desired references generated by a guidance system. The state $\hat{b}_f$ is a lowpass-filtered state of the bias estimate $\hat{b}$,

$$\dot{\hat{b}}_f = -T_f^{-1}(\hat{b}_f - \hat{b}), \quad (16)$$

where T_f is a diagonal matrix of the filter time constants. This filter was used instead of the bias estimate directly, to achieve a calmer control signal; see [10] for more details. The tuning for the observer and controller gains were found through trial and error.

1) EXPERIMENTAL CLOSED-LOOP RESULTS

The vessel followed the DP 4-corner maneuver described in Section V-B, and Figure 4 shows the response of the vessel for two different runs. The left side of the figure shows the North/East position of the target and the two runs, and the right side of Figure 4 shows the heading setpoint and the vessel heading for the two runs. The figure indicates that the observer worked well in closed loop, and vessel followed the maneuver well. The best performance was in surge, and when the degree of coupling between surge, sway, and yaw increased, tracking the reference was harder.

The two runs had similar environmental conditions, with current of velocity 0.3 m/s and direction 300°, and with wind speed of 6 m/s and direction 250°. For both runs the observer gains were the same, but the filter time constant for the bias was four times higher for run 2. As seen from Figure 4, both runs were quite similar in performance, but run 2 was more oscillatory, at least on the last part of the maneuver. This is probably due to the higher bias filter time constant. The closed-loop results indicate that the observer worked well in closed loop, and managed to control the vessel to a satisfactory degree.

F. OBSERVER WITH TIME-VARYING BIAS AND VELOCITY INJECTION GAINS

We now present the results for the time-varying observer in (3), where both $K_3(t)$ and $K_4(t)$ are time-varying. In addition, the results of the observer in [10] with only $K_3(t)$ time-varying is presented, with $K_4 = K_{4,min}$. Two benchmarks are included to compare the performance of the observers. The first benchmark is an observer that always uses $K_{3,min}$

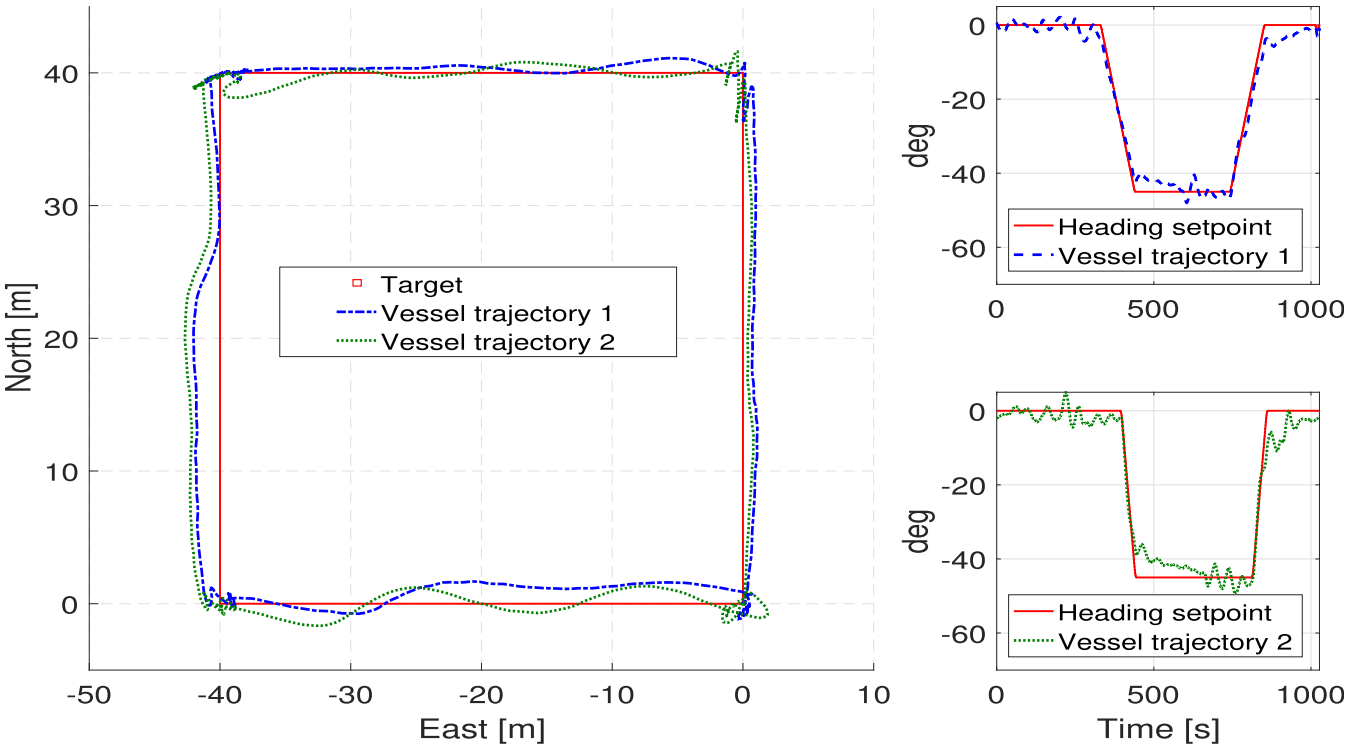

FIGURE 4. Full-scale experimental verification on R/V Gunnerus of the algorithm from [10]. The left plot shows the four corner target and results of two different runs. The right side shows the heading setpoint and the response of the two different runs.

and $K_{4,min}$ in (4), named the *baseline* observer, working well in steady state. This is the "nonlinear passive observer" presented in [16], with normal tuning, and is typical in the literature. The second benchmark is an observer called the *aggressive* observer that always uses $K_{3,max}$ and $K_{4,max}$, working well in transients.

1) TUNING

To find the tuning for the observers, derivative free optimization, as discussed in Section V-D, was used with the cost function

$$J = J_\eta + c_v J_v, \tag{17}$$

where J_η and J_v are defined in (14a) and (14b), and c_v is a scaling factor to weight the relative contributions for position and velocity.

For the simulated data in Section V-F.2, a maneuver with many transients has been used. The data set has both a change of the current direction and a heading change combined with a North/East position change, with short time intervals between the transients. The resulting tuning was adjusted to accommodate the stability requirements in (11), and this was used as a guide to tune the transient observer gains, that is, the maximum values of $K_3(t)$ and $K_4(t)$.

In order to find values for $K_{3,min}$ and $K_{4,min}$, several tests have been conducted. We tried to select maximum gains higher than the gains from the tuning found from DFO and combined this with a low minimum tuning, but this did not yield good results. This makes sense as the DFO tuning is found over a lot of transients, and thus is very aggressive already.

Thereafter, using the DFO tuning as the maximum values, we searched though several variations for the minimum tuning. Setting the minimum gains to $60-70\%$ of the maximum gains yielded the best results. However, since we needed to adjust $K_{3,max}$ to satisfy the stability requirements in (11), we selected the highest feasible $K_{3,max}$ that in combination with minimum gains $K_{i,min} = 0.7\ K_{i,max}$ that satisfied (11). This gave $K_{3,max} = 0.5\ K_{3,max}^{DFO}$.

For the full-scale experimental data, a similar approach was used where the DP 4-corner maneuver seen in Figure 3 was used to find the transient tuning. To find the gains by using DFO, the post-processed position measurement and velocities were used. The velocities were found by differentiating the North/East position and heading using a finite impulse response (FIR) filter. A search over possible ratios between the maximum and minimum tuning was performed, where 0.7 performed well, satisfying (11) with $K_{3,max} = 0.5\ K_{3,max}^{DFO}$.

2) ESTIMATION BASED ON SIMULATED DATA

For the simulated data the vessel is controlled by (15) and (16) that operate on the estimated states, i.e. the observers operate in closed loop.

In the data series, the current changes direction at $t = 500$ seconds, and at $t = 1000$ seconds there is

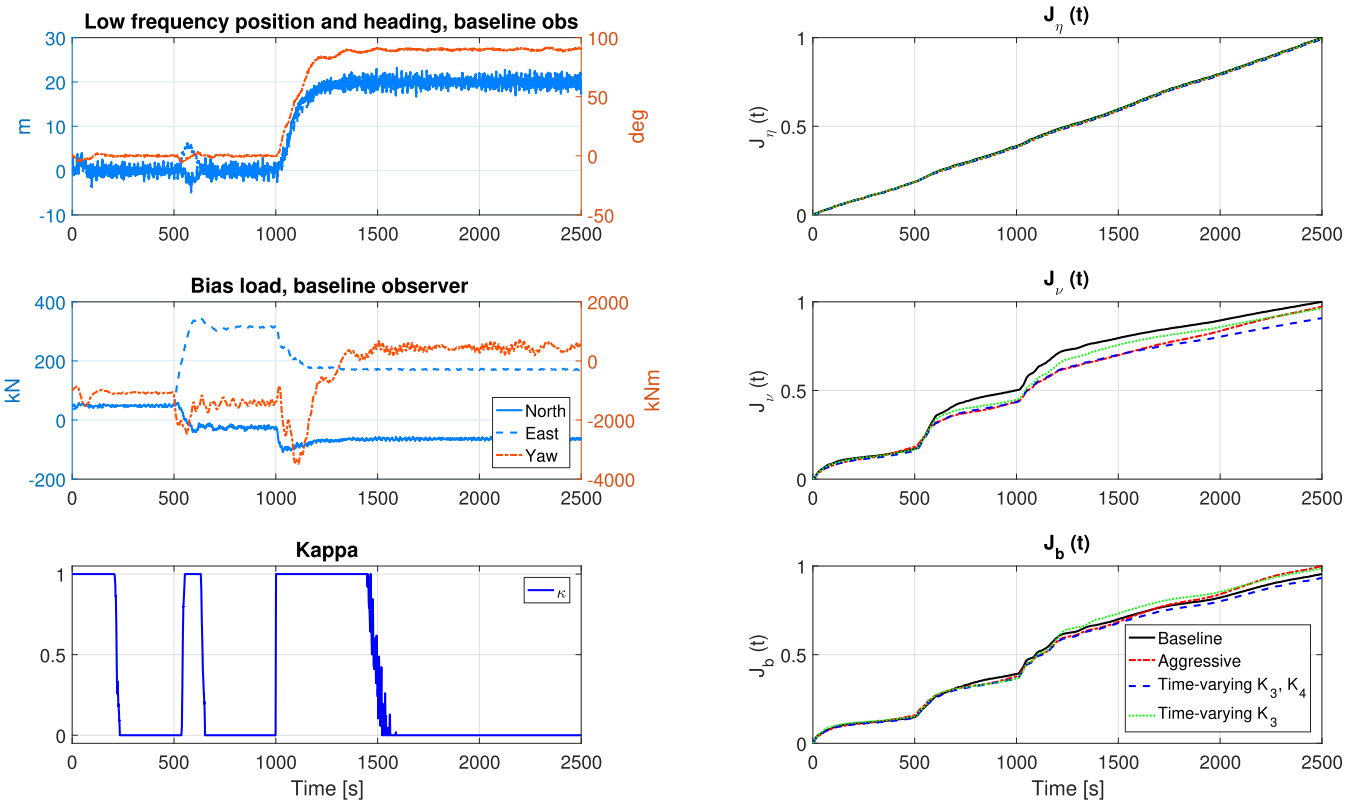

FIGURE 5. Simulation results of observer in closed-loop.

TABLE 3. Performance indices for the estimation error, simulation data.

Time:	0-1500 s			2000-3500 s		
Observer	J_η	J_ν	J_b	J_η	J_ν	J_b
Baseline	2125.2	96.4	666.8	2125.6	36.3	355.0
Aggressive	2098.8	84.7	653.2	2141.8	50.0	446.9
Time-varying K_3 and K_4	2099.3	85.1	646.2	2125.6	36.3	351.3
Time-varying K_3	2117.2	91.7	697.1	2125.6	36.4	352.4

a setpoint change of both North/East position and heading. Figure 5 shows the results of the four observers. The left side shows the low-frequency North/East position and heading of the baseline observer in the top plot, the middle plot shows the bias load of the baseline observer, found by solving (1d) for b, and the lower left plot shows the κ variable of the observer with time-varying $K_3(t)$ and $K_4(t)$ from (4). The right side shows the performance indices J_η, J_ν, and J_b in (14) from top to bottom, respectively. The same performance index values for 0 to 1500 seconds and for the steady-state time interval 2000 to 3500 are listed in Table 3. Note that the steady-state time interval 2500 to 3500 seconds is not shown in Figure 5.

Looking at the left side of Figure 5 we see that the bias loads change a lot, both at the current direction change at 500 seconds, and at the setpoint change at 1000 seconds. The κ-value starts at 1 due to high initialization of $\tilde{\eta}_f(t)$ in (5b) in order to handle initial transients before settling at $\kappa = 0$. At the heading change at 1000 seconds, κ reacts quickly and jumps to 1 due to the non-zero desired yaw rate. The current direction change at 500 seconds has to be detected through deterioration of the observer performance and the subsequent rise in $|\tilde{\eta}_f(t)|$. Therefore it takes κ longer to reach 1 during the current direction change.

On the right side of Figure 5 and in Table 3 we see that all observers perform similarly for J_η. In both the estimation of the velocity and bias loads, the time-varying observer proposed in this paper performs the best, especially in velocity. It outperforms the aggressive observer due to effect of lower oscillations in steady state, and it outperforms the baseline due to faster reaction over the transients. The time-varying observer with only K_3 time varying performs worse than the observer with both K_4 and K_3 time varying, but it performs better than the baseline observer in transients. As seen from Table 3, the baseline and time-varying observers are slightly better than the aggressive observer in steady state for position estimation, and considerable better for bias and velocity estimation.

If the noise variance of the measurements is increased, the time-varying observer performs better relative to the aggressive, due to lower tuning in steady state. To make the time-varying setup better handle large measurement noise, we could make ε_η in (5) depend on the variance of the noise. In this way the time-varying observer could adopt lower gains if the measurement noise increases.

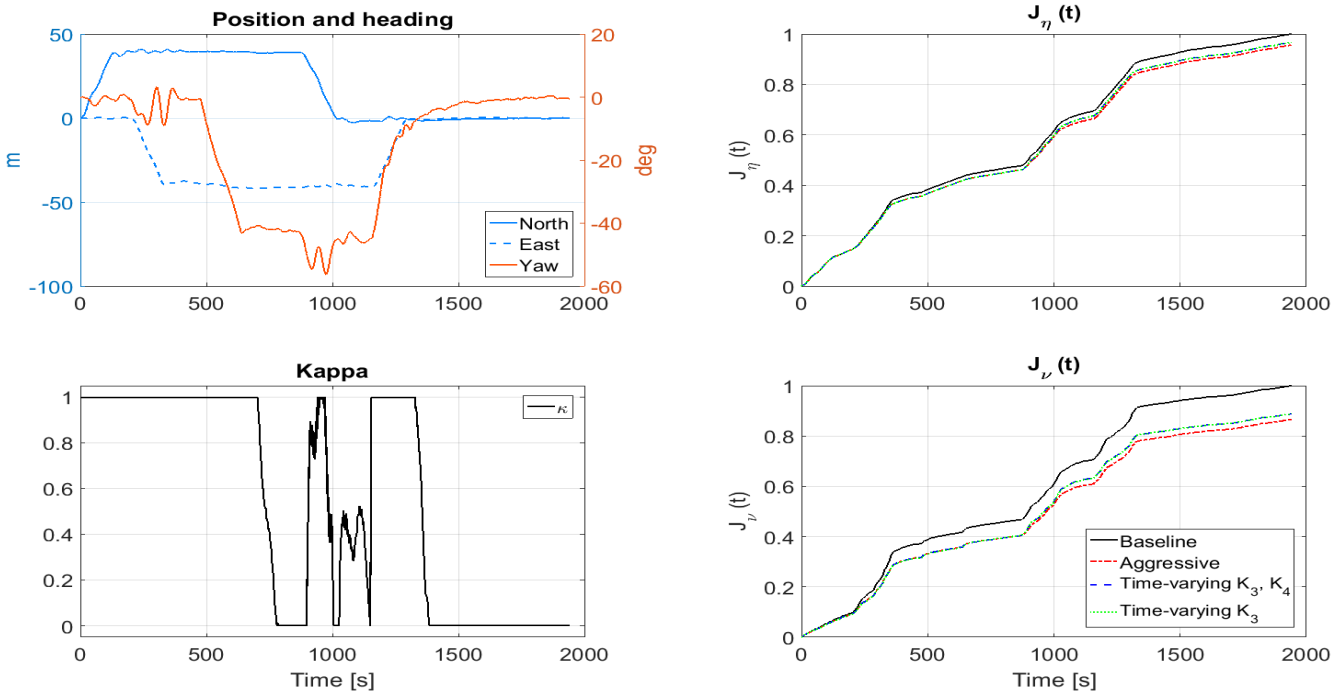

FIGURE 6. Observer results on full-scale experimental data from a DP 4-corner maneuver with R/V Gunnerus.

TABLE 4. Performance indices for the estimation error, full-scale exp. data.

Time:	0-1500 s		1500-1940 s	
Observer	J_η	J_ν	J_η	J_ν
Baseline	142.09	144.02	10.97	8.95
Aggressive	135.27	123.35	11.02	9.05
Time-varying K_3 and K_4	137.00	126.94	10.97	8.95
Time-varying K_3	138.83	126.97	10.97	8.95

3) ESTIMATION BASED ON FULL-SCALE MEASUREMENTS

Figure 6 shows the results of the four observers on data from R/V Gunnerus from ADPRC 2016. In the data set presented, the vessel is exposed to a current roughly estimated to 0.6 m/s and direction 170°, and with wind speed 5 m/s and direction 150°. The left side of the plot shows the measured North/East position, and heading in the top plot. The bottom left plot shows the κ variable. Notice that κ is 1 for most of the four corner maneuver, and after 1500 a steady state is reached.

Since the four corner maneuver has a lot of transients, and not too much steady state, it is harder to show a difference between the different observers. The right side of Figure 6 shows the performance indices J_η and J_ν in (14), and all four observers perform similarly for J_η, but for J_ν the baseline observer is significantly worse than the other three, due to all the transients. However, the performance between the observer with only time-varying K_3 to that of the other time-varying observer is smaller than for the closed-loop simulation results. The values for J_η and J_ν for the transient and steady state periods are given in Table 4, and the trend is similar to that of the closed-loop simulation results, although the differences in steady state are smaller. This is natural as the steady state in simulation is actually steady, and here the environment is changing, and there is less time to settle into steady state conditions.

VI. CONCLUSION

A time-varying model-based observer with good performance in both transients as well as steady state has been proposed. The observer is shown to be UGES, and performance is shown through a simulation study and on full-scale experimental data. In addition, a full-scale closed-loop verification is presented, and this shows that the observer works to a satisfactory degree in closed loop. Satisfactory transient tuning for the observer is found through derivative free optimization. The time-varying observer shows a marginal benefit over a well-tuned transient observer, depending on variations in measurement noise and environmental conditions. Especially, if there are large periods of steady state in between transients the time-varying observer is a tractable solution over the conventional DP observer. In addition, the added complexity of implementation for the time-varying gains is very small.

ACKNOWLEDGEMENTS

The authors would like to thank the crew of R/V Gunnerus and the personel from Kongsberg Maritime for their help and support during the sea trials. Especially, they would like to thank Rune Skullestad and Øystein Lurås from Kongsberg Maritime for help with code implementation and the simulation platform to test our code. Also, they would like to thank the NTNU research team, Øivind K. Kjerstad, Asgeir J. Sørensen, Mikkel E. N. Sørensen, Zhengru Ren, and

Morten Breivik. Finally, MSc. student Alexander Mykland deserves a thanks for writing the test log.

REFERENCES

[1] International Maritime Organization. "Guidelines for vessels with dynamic positioning systems," International Maritime Organization, London, U.K., Tech. Rep. MSC/circ.645, 1994.
[2] T. I. Fossen, *Handbook Marine Craft Hydrodynamics Motion Control*. Hoboken, NJ, USA: Wiley, 2011.
[3] A. J. Sørensen, "A survey of dynamic positioning control systems," *Annu. Rev. Control*, vol. 35, no. 1, pp. 123–136, Apr. 2011.
[4] J. E. G. Refsnes, "Nonlinear model-based control slender body AUVs," Ph.D. dissertation, Dept. Marine Technol., Norwegian Univ. Sci. Technol., Trondheim, Norway, 2007.
[5] O. K. Kjerstad and R. Skjetne, "Disturbance rejection by acceleration feedforward for marine surface vessels," *IEEE Access*, vol. 4, pp. 2656–2669, 2016.
[6] T. H. Bryne, T. I. Fossen, and T. A. Johansen, "Nonlinear observer with time-varying gains for inertial navigation aided by satellite reference systems in dynamic positioning," in *Proc. 22nd Medit. Conf. Control Autom. (MED)*, Jun. 2014, pp. 1353–1360.
[7] D. J. Belleter, D. A. Breu, T. I. Fossen, and H. Nijmeijer, "A globally k-exponentially stable nonlinear observer for the wave encounter frequency," in *Proc. IFAC Conf. Control Appl. Marine Syst.*, 2013, vol. 46. no. 33, pp. 209–214.
[8] D. J. W. Belleter, R. Galeazzi, and T. I. Fossen, "Experimental verification of a global exponential stable nonlinear wave encounter frequency estimator," *Ocean Eng.*, vol. 97, pp. 48–56, Mar. 2015.
[9] S. A. Værnø and R. Skjetne, "Hybrid control to improve transient response of integral action in dynamic positioning of marine vessels," in *Proc. IFAC Conf. Manoeuvring Control Marine Craft*, 2015, vol. 48. no. 16, pp. 166–171.
[10] S. A. Værnø, A. H. Brodtkorb, R. Skjetne, and A. J. Sørensen, "An output feedback controller with improved transient response of marine vessels in dynamic positioning," in *Proc. IFAC Conf. Control Appl. Marine Syst.*, 2016, vol. 49. no. 23, pp. 133–138.
[11] R. Skjetne *et al.*, "Amos dp research cruise 2016: Academic full-scale testing of experimental dynamic positioning control algorithms onboard RV gunnerus," in *Proc. ASME 36th Int. Conf. Ocean, Offshore Arctic Eng.*, 2017, pp. 1–4.
[12] P. Fung and M. J. Grimble, "Dynamic ship positioning using a self-tuning Kalman filter," *IEEE Trans. Autom. Control*, vol. 28, no. 3, pp. 339–350, Mar. 1983.
[13] M. Katebi, I. Yamamoto, M. Matsuura, M. Grimble, H. Hirayama, and N. Okamoto, "Robust dynamic ship positioning control system design and applications," *Int. J. Robust Nonlinear Control*, vol. 11, no. 13, pp. 1257–1284, 2001.
[14] E. Tannuri and H. Morishita, "Experimental and numerical evaluation of a typical dynamic positioning system," *Appl. Ocean Res.*, vol. 28, no. 2, pp. 133–146, 2006.
[15] A. J. Sørensen, "Marine control systems—Lecture notes," Dept. Marine Technol., Dept. Marine Technol., Norwegian Univ. Sci. Tech., Trondheim, Norway, 2013.
[16] T. I. Fossen and J. P. Strand, "Passive nonlinear observer design for ships using Lyapunov methods: Full-scale experiments with a supply vessel," *Automatica*, vol. 35, no. 1, pp. 3–16, Jan. 1999.
[17] K.-P. Lindegaard, "Acceleration feedback dynamic positioning," Ph.D. dissertation, Dept. Eng. Cybern., Norwegian Univ. Sci. Technol., Trondheim, Norway, 2003.
[18] T. I. Fossen and T. Perez. (2010). *Mss. Marine Systems Simulator*, accessed on Feb. 2015. [Online]. Available: http://www.marinecontrol.org
[19] W. G. Price and R. E. D. Bishop, *Probabilistic Theory of Ship Dynamics*. New York, NY, USA: Halsted, 1974.

SVENN ARE VÆRNØ was born in Norway in 1990. He received the M.Sc. degree in marine technology from the Norwegian University of Science and Technology, Trondheim, Norway, in 2014, where he is currently pursuing the Ph.D. degree with the Norwegian Centre of Excellence Autonomous Marine Operations and Systems. His research include marine motion control systems and dynamic positioning.

ASTRID H. BRODTKORB received the M.Sc. degree in marine technology from the Norwegian University of Science and Technology, Trondheim, in 2014, where she is currently pursuing the Ph.D. degree in marine control systems with the Norwegian Centre of Excellence Autonomous Marine Operations and Systems. Her main research interests are hybrid control theory, observers, and sea state estimation applied to dynamic positioning systems for marine vessels.

ROGER SKJETNE received the M.Sc. degree in control engineering from the University of California at Santa Barbara in 2000, and the Ph.D. degree from the Norwegian University of Science and Technology (NTNU), in 2005. Prior to his studies, he was an Electrician with Aker Elektro AS on numerous oil installations for the North Sea. From 2004 to 2009, he was with Marine Cybernetics AS, where he was involved in hardware-in-the-loop simulation for testing safety-critical marine control systems. He was the Project Manager for the KMB Arctic DP Research Project. Since 2009, he has held the Kongsberg Maritime Chair of Professor in marine control engineering with the Department of Marine Technology, NTNU, where he is currently the Leader of the Research Group on Marine Structures. He is the Leader of the Ice Management Work Package with the CRI Sustainable Arctic Marine and Coastal Technology, an Associated Researcher with the CoE Center for Ships and Ocean Structures and CoE Autonomous Marine Operations and Systems, and a Principal Researcher with the CRI on Marine Operations. He is also a Co-Founder of the two companies BluEye Robotics and ArcISo. His research interests are within Arctic station keeping operations and ice management systems for ships and rigs, environmentally robust control of shipboard electric power systems, and nonlinear control theory for motion control of single and groups of marine vessels. He received the Exxon Mobil Prize for best Ph.D. thesis in applied research for his Ph.D. thesis at NTNU.

VINCENZO CALABRÒ (M'10) was born in Messina, Italy, in 1982. He received the Ph.D. degree in robotics automation and bioengineering from the University of Pisa, Italy, in 2012. In 2012, he joined the Cybernetics Research and Development Group, Kongsberg Maritime, where he developed and improved industrial solutions for Dynamic Positioning systems and related applications. Since 2017, he has been the Research and Development Manager with Norwegian Subsea AS company, developing inertial-based systems and applications. His current research interests include state observer design, neural networks, model predictive control, non-linear control, and fuzzy logic.